High-temperature elastic properties of a nickel-based superalloy studied by surface Brillouin scattering

2001 J. Phys.: Condens. Matter 13 2281

(http://iopscience.iop.org/0953-8984/13/10/320)

INSTITUTE OF PHYSICS PUBLISHING JOURNAL OF PHYSICS: CONDENSED MATTER

J. Phys.: Condens. Matter **13** (2001) 2281–2294 www.iop.org/Journals/cm PII: S0953-8984(01)18098-7

High-temperature elastic properties of a nickel-based superalloy studied by surface Brillouin scattering

X Zhang, P R Stoddart, J D Comins and A G Every

Department of Physics, University of the Witwatersrand, Johannesburg, Wits 2050, South Africa

Received 18 October 2000, in final form 12 January 2001

Abstract

Surface Brillouin scattering (SBS) has been used to study the thermally induced surface vibrations (phonons) and thereby obtain the elastic properties of the nickel-based superalloy CMSX-4. SBS spectra have been acquired for a range of wavevector directions in the (001) surface in the single-crystal specimen to determine the angular variation of SAW velocities and the nature of the various excitations. Rayleigh and pseudo-surface acoustic waves as well as the details of the Lamb shoulder are studied, and the elastic constants and engineering moduli are determined using different, but self-consistent, methods at ambient and high temperatures. Calculations of the SBS spectra using surface Green function methods are in good agreement with the experimental results.

1. Introduction

The components of gas turbine engines are exposed to extreme conditions of high temperature, corrosive gases, vibration, high mechanical loads and low-cycle fatigue. The advanced nickel-based superalloys meet these stringent demands, retaining useful strength at temperatures as high as 1000 °C. The high-temperature capability and properties of these superalloys have been further improved by growing them as single crystals, making them the most suitable materials for high-performance gas turbine airfoil blades [1, 2].

The very interesting microstructure of nickel-based superalloys (nominally Ni_3Al but with a significant admixture of other elements) is the key to their outstanding creep resistance and high-temperature properties. Compositionally ordered fcc domains (called the γ' phase) are embedded in a disordered fcc matrix (the γ phase). Complex heat treatments are needed to obtain the optimal size and volume fraction of the ordered γ' cuboids for high temperature strength and stability. Both γ and γ' phases form a single crystal in the sense that, in their alignment, they share a common Bravais lattice.

The elastic constants of certain nickel-based superalloys have been measured previously by various means [3–5]. The present work, using surface Brillouin scattering, was performed on a single crystal nickel-based cubic superalloy (CMSX-4). There is considerable interest in the high-temperature elastic properties of such materials [1]. The full set of elastic constants of this anisotropic material allow the Young's modulus, the shear modulus and Poisson's ratio to

be calculated in any direction, these being required in the design of statically and dynamically loaded components.

Surface Brillouin scattering of opaque solids is concerned with the study of thermally induced surface vibrations in the GHz frequency range and has been reviewed by Nizzoli and Sandercock [6], Mutti *et al* [7] and Comins [8]. Analysis using surface Green's functions (see Zhang *et al* [9] for a detailed treatment) permits the evaluation of the elastic constants in a variety of situations, including bulk solids, thin films and multi-layers. The technique has recently been extended to high temperatures by Stoddart *et al* [10, 11] and to high pressures by Crowhurst *et al* [12]. In certain cases (e.g. Mendik *et al* [13], Stoddart *et al* [11]) it has proved possible to extract complete sets of elastic constants for single crystals by fitting the angular dispersion of surface acoustic waves (SAWs). This approach is not universally successful and can lead to substantial uncertainties in particular elastic constants even though the materials may be highly elastically anisotropic. The article by Sklar *et al* [14], in the context of acoustic microscopy, provides a critical analysis, including the stability of solutions and quality of fit to the data.

In the present work we establish unambiguous values of the elastic constants of the superalloy CMSX-4 both at ambient and high temperatures by using a combination of angular dispersion of SAWs together with the thresholds of the Lamb shoulder in SBS spectra (Mock and Güntherodt [15], Comins [8]). The latter feature results from light scattering from the surface displacements of the continuum of bulk waves. We also examine the form of the Lamb shoulder as a function of the direction of the surface wavevector in considerable detail, and compare the experimental results with calculations in order to identify and understand the features. Brief preliminary accounts of this work appear in [8] and [16].

2. Theoretical aspects

The back-scattering geometry used in SBS is described in figure 1 and leads via wavevector conservation to the relation $q_{//} = 2k_i \sin\theta_i$. θ_i is the incident angle, k_i is the wavevector of the incident light while $q_{//}$, $V = \omega/q_{//}$ and ω are respectively the wavevector, velocity and angular frequency of the surface acoustic excitation. For a chosen incident wavelength of light, the angle of incidence θ_i establishes $q_{//}$, and the measurement of ω, by the frequency shift of the scattered light, determines V. Rotation of the sample about the surface normal by a given angle α from a chosen symmetry direction (e.g. from the [100] direction on the (001) plane in a cubic material) permits the angular variation of the SAW velocities to be studied. The backscattering geometry has been discussed in detail by Stoddart *et al* [17] in relation to measurement precision in SBS measurements.

The SBS spectra of highly opaque solids, mediated by surface ripple scattering are conveniently calculated by the surface Green's function method as discussed in detail by Zhang *et al* [9]. In brief, for chosen values of ω and $\boldsymbol{q}_{//}$, the scattering efficiency or cross section $I(\omega)$ at temperatures $T \gg \hbar\omega/k_B$ is proportional to the power spectrum of the normal displacements $u_3(0)$ of the surface with that wavevector and at that frequency. In turn, the power spectrum is related to G_{33}, the (x_3, x_3) component of the Fourier (frequency and wavevector) domain elasto-dynamic Green's function evaluated at surface. Accordingly,

$$I(\omega) = A\frac{T}{\omega}\mathrm{Im}\,\{G_{33}(q_{//}, x_3 = 0, \omega + \mathrm{i}0)\} \tag{1}$$

where A is a constant that depends on the properties of the medium, the scattering geometry, and the frequency and polarization of the incident light.

The method of calculation of G_{33} uses the method of partial waves that satisfy the appropriate boundary conditions. The partial waves having polarization vectors $U_i^{(n)}$

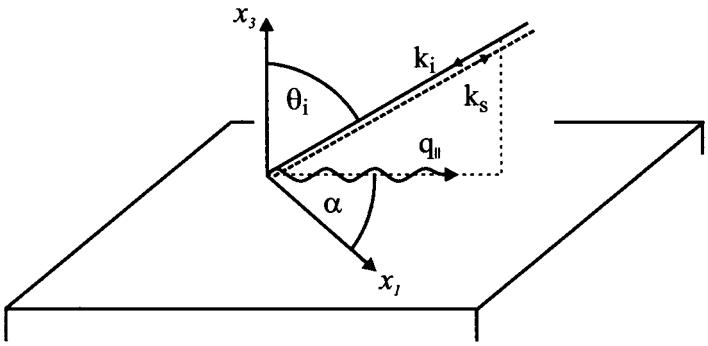

Figure 1. Backscattering geometry for surface Brillouin scattering.

correspond to different wavevector components $q_3^{(n)}$ perpendicular to the free surface and are real or complex solutions of the sextic Christoffel characteristic equation. Only the three outgoing plane waves ($n = 1, 2, 3$) are retained as discussed in Farnell [18]. The outgoing waves are either homogeneous with $q_3^{(n)}$ real and having ray vectors $\boldsymbol{V} = \partial\omega/\partial\boldsymbol{q}$ directed into the interior of the solid, or evanescent waves with Im $(q_3^{(n)}) > 0$, and having amplitudes that decrease into the interior. The boundary conditions on the surface tractions and displacements yield the partial wave amplitudes. The Green function is obtained as a linear combination of these partial waves, namely

$$G_{33}(q_{//}, \omega) = \sum_{n=1}^{3} \frac{\mathrm{i}}{\omega} (\boldsymbol{B}^{-1})_3^n U_3^{(n)} = \sum_{n=1}^{3} \frac{\mathrm{i}}{\omega} \frac{\mathrm{adj}(\boldsymbol{B})_3^{(n)}}{|\boldsymbol{B}|} U_3^{(n)} \tag{2}$$

in which

$$B_l^{(n)} = \sum_{pq} C_{3lpq} U_p^{(n)} q_q^{(n)} / \omega. \tag{3}$$

Equation (3) represents the relationship between the boundary condition determinant $|\boldsymbol{B}|$ and the elastic properties of the material expressed in terms of the elastic constant tensor C_{ijkl}.

The nature of the excitations depends on the real or complex values of the wavevectors $q_3^{(n)}$ of the partial waves. For SAW frequencies lower than that corresponding to the transverse bulk wave threshold, or transonic state, the three partial wave solutions all have complex $q_3^{(n)}$. The superposition of these phase-matched evanescent waves results in the Rayleigh wave (RW), a true surface wave whose amplitude falls essentially to zero within a few wavelengths from the surface and which corresponds to a zero value of the boundary value determinant $|B|$.

Bulk acoustic waves that have a component of displacement normal to the surface also contribute to the SBS spectrum. In the frequency range beyond the longitudinal wave threshold, all contributing modes, transverse and longitudinal are propagating bulk waves with real $q_3^{(n)}$. For frequencies between the transverse and longitudinal thresholds there is a mixture of modes with both complex and real values of $q_3^{(n)}$. The contribution of these waves in both cases leads to a continuous band of excitations in which the longitudinal (L) and transverse (T) thresholds can be identified. These limiting bulk waves correspond to ray vectors parallel to the surface and are described as lateral waves. The limiting frequencies in respect of the continuum of excitations from the bulk modes (Lamb shoulder) are thus $\omega_T = V_T q_{//}$ for the transverse threshold (transonic state), $\omega_L = V_L q_{//}$ for the longitudinal threshold, while for the RW, $\omega_R = V_R q_{//}$. Measurement of the frequencies and hence the velocities corresponding to the respective thresholds for the surface wavevector in given high symmetry directions can

Table 1. Nominal composition in mass per cent of CSMX-4 superalloy [1].

Ni	Cr	Co	Mo	W	Ta	Al	Ti	Re	Hf
Balance	6.5	10	0.6	6.0	6.0	5.6	1.0	3.0	0.1

enable the complete set of elastic constants to be obtained. For the (001) plane of the cubic crystal used the present work, in respect of the [110] direction, $V_L = [(c_{11}+c_{12}+2c_{44})/2\rho]^{1/2}$, while for the [100] direction $V_L = (c_{11}/\rho)^{1/2}$, with no explicit solutions for the Lamb shoulder thresholds. Besides the surface excitations discussed above, the Green's function formalism is successful in reproducing the sharp resonance that may exist for directions close to [110] on the (001) surface of certain cubic materials. The frequency of this resonance lies within in the continuum of bulk wave excitations between the slow transverse and fast transverse wave thresholds. Two of its partial waves are evanescent while the third has a bulklike nature. The wave, designated a pseudo-SAW (p-SAW), retains a considerable surface character, but the energy losses to the bulk reduce its lifetime in comparison with the RW. Exactly in the [110] symmetry direction it becomes a two component true surface wave. The angular dispersion of the p-SAW provides addition data for the purpose of fitting the dispersion curves.

3. Experimental details

The CMSX-4 superalloy specimen was supplied by the Division of Materials Science and Technology, CSIR, Pretoria. The elemental composition of this superalloy is shown in table 1. The sample had been solution heat-treated at temperatures up to 1310 °C for 8 h to optimize the microstructure. This was followed by a rapid quench with pressurized argon, but no aging heat treatment was performed.

A sample was cut from the larger specimen supplied using a low-speed diamond saw and oriented by means of Laue x-ray backscattering. The sample was sequentially lapped on a SiC grinding disc and examined by X-rays until the [001] direction was within one degree of the surface normal. A second face was ground parallel to the first and the sample reduced to a rectangular cross section of approximately 3.8×3.3 mm^2. A high-quality surface was then prepared for the SBS measurements by polishing on 1 μm and 0.1 μm diamond impregnated discs.

A description of the experimental arrangement used for the SBS measurements is given in Comins [8]. Light of wavelength 514.5 nm, generated by an argon ion laser operated in a single axial mode, was focused onto the sample and by a 120 mm focal length lens with relatively small aperture of $f/5.5$ in a backscattering arrangement. The scattered light was analysed by a Sandercock (3 + 3) pass tandem Fabry–Pérot interferometer fitted with a JRS vibration isolation system and measured by an SPCM-PQ detector based on a low-noise, high-sensitivity silicon avalanche diode. The scattering angle $\theta_s = \theta_i$ used in the experiments was 70.7°, determined by the geometry of the optical furnace and matched in the room-temperature experiments. The scattering cross section for p–p scattering (polarization in the sagittal plane) is close to a maximum for this value of the scattering angle. Stoddart *et al* [17] have provided a detailed analysis of the effects of a finite collection aperture, scattering out of the sagittal plane and variations of the scattering cross section with scattering angle, on distortions in the measured SBS spectra. The analysis shows that negligible errors from these effects occur with the present experimental conditions and no corrections to the data were considered necessary.

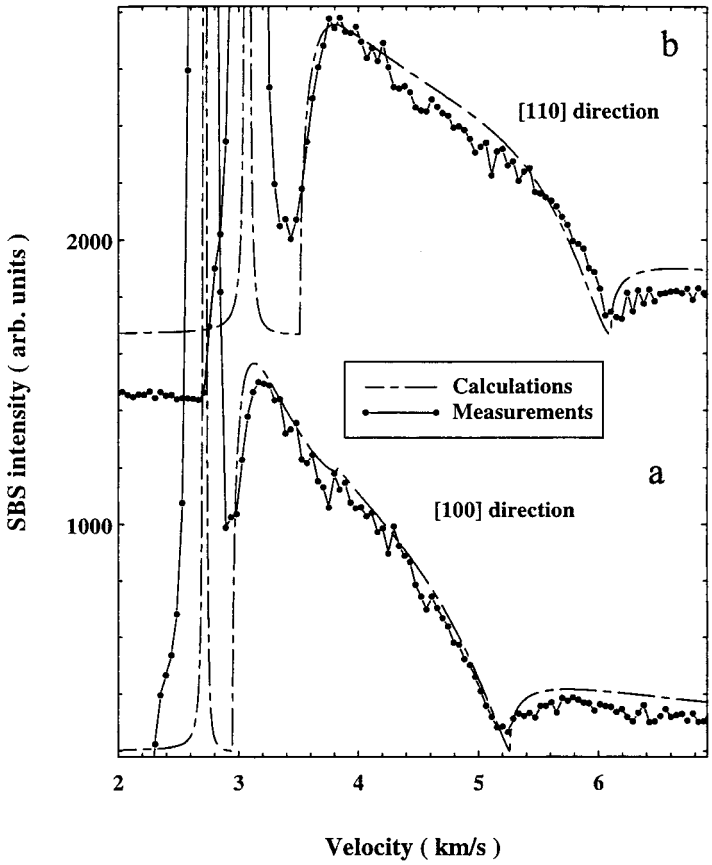

Figure 2. The measured and calculated SBS spectra for the respective [100] and [110] surface wavevector directions ($\alpha = 0^\circ$ from [100] in (a) and $\alpha = 45^\circ$ from [100] in (b)) on the (001) plane of CMSX-4. The upper graph has been displaced for reasons of clarity.

4. Results

4.1. Room-temperature measurements

SBS spectra were measured for a range of the angle α on the (001) surface of the CMSX-4 superalloy. In each case α was measured from the [100] direction. On this surface there are two wave branches: the Rayleigh SAW and the pseudo-SAW (p-SAW) as discussed in section 2. Owing to the large anisotropy of CMSX-4, it is possible to observe the two SBS peaks simultaneously in certain directions. The Rayleigh peak is dominant in the range of surface wavevector directions α in the interval 0° to 25° (e.g. figure 2(a) for $\alpha = 0^\circ$), remains visible in the crossover region from 25° to 30° (e.g. figure 3(a) for $\alpha = 28^\circ$) and vanishes as the Rayleigh wave ultimately degenerates into the slow transverse bulk wave at $\alpha = 45^\circ$, yielding no normal surface displacements. The p-SAW, also being visible in the crossover region, dominates in the range of α values from 30° to 45° (e.g. figure 3(b) for $\alpha = 40^\circ$ and figure 2(b) for $\alpha = 45^\circ$). Other features in these diagrams and the comparison of experimental measurements and theoretical calculations will be discussed later.

In order to determine the angular dependence of the SAW velocities on the (001) plane it is necessary to accurately align the laser beam with the chosen [100] symmetry direction in

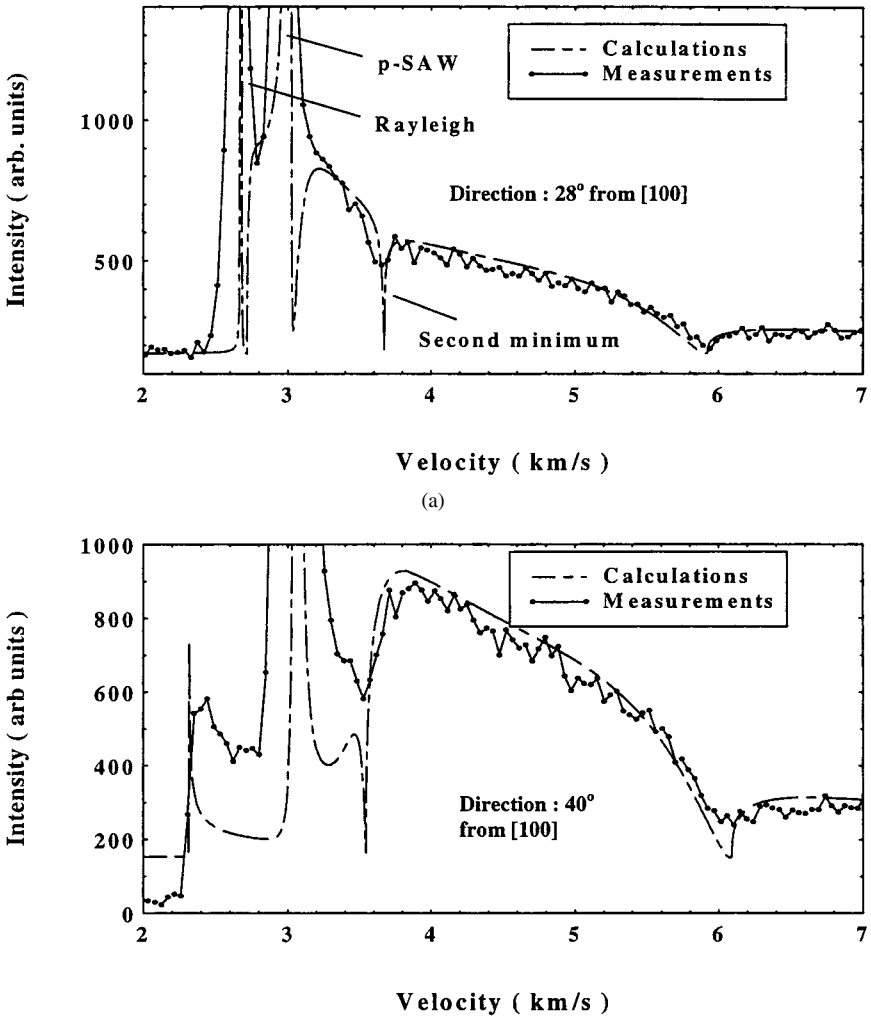

Figure 3. The measured and calculated SBS spectra for surface wavevector directions $\alpha = 28^\circ$ from [100] in (a) and $\alpha = 40^\circ$ from [100] in (b) on the (001) plane in CMSX-4. The abrupt decrease in intensity below 2.4 km s^{-1} in the experimental spectrum in (b) arises from the slow-scanning window.

the crystal. As discussed in section 3 the symmetry directions in the crystal were identified by Laue x-ray backscattering. However, visual alignment is insufficiently accurate and a different procedure was adopted. A series of measurements were performed over a wide range of the angle α and the angular variation of the SAW velocity was determined. By fitting a simple cosine function to the data for the Rayleigh SAW near where it is most prominent, the [100] direction was established to within 2°. Once this direction was determined, a measurement of the range of α angles between the [100] and [110] directions revealed the full velocity profile of the surface.

The velocities of both the Rayleigh SAW and the p-SAW are strongly direction dependent on the (001) plane as is shown by their angular dispersion in figure 4; as a result of the sample

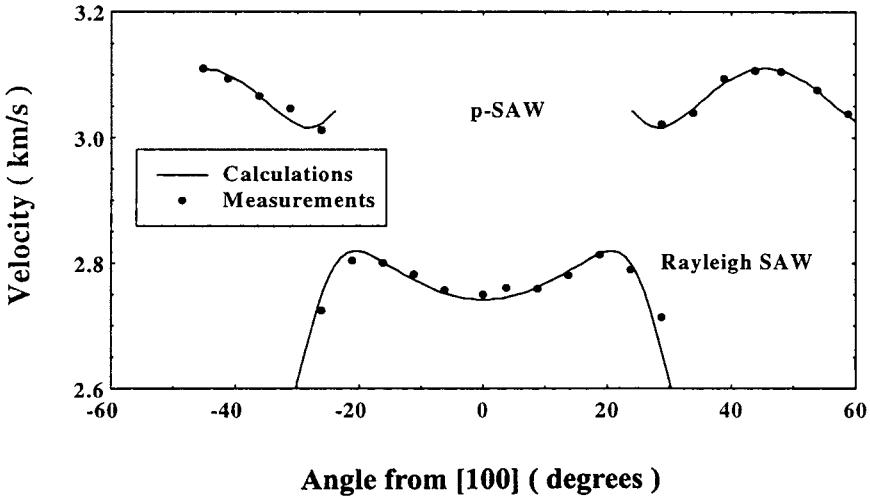

Figure 4. The angular dependence of the Rayleigh SAW and p-SAW velocities on the (001) surface of CMSX-4 at room temperature.

alignment the expected symmetry is clearly evident. The phase velocity of the Rayleigh SAW near the [100] direction is about 2.75 km s^{-1} and increases as the surface wavevector moves from [100], attaining a maximum value of 2.81 km s^{-1} in a direction near 20° from [100]. Thereafter the Rayleigh SAW velocity decreases rather steeply and its intensity diminishes rapidly. The phase velocity of the p-SAW is higher than that of the Rayleigh SAW. It is first observed in the region 25°–30° where its velocity is about 3.05 km s^{-1}, steadily increases in velocity with increasing values of φ and achieves a maximum value of about 3.15 km s^{-1} in the [110] direction. The appearance of the spectra over the range of angles α is provided by figures 2 and 3.

4.2. Recovery of the elastic constants

4.2.1. Use of the angular dispersion of surface acoustic waves. CMSX-4 is a highly elastically anisotropic material (anisotropy ratio $A \cong 2.8$). With the strongly direction dependent values of the SAW and p-SAW velocities on the (001) surface, as determined from the positions of the frequency maxima of the respective SBS peaks, it was initially expected that these data alone would permit the extraction of the set of elastic constants by the procedure employed previously [11, 13]. The process of fitting the SAW dispersion is one of inversion. The minimization of $\chi^2 = \sum_{SAWs}(V_i^{meas} - V_i^{calc})^2$ with respect to variations of the elastic constants was carried out, where the V_i^{calc} are the respective velocities determined from the surface Green function for the Rayleigh SAW and the p-SAW and V_i^{meas} are the measured values of the velocities of these SAWs by SBS, using in each case the position of the frequency maximum.

In practice, however, the velocity dispersion data of both the Rayleigh and the p-SAW were not able to determine c_{11} or c_{12} individually. As an illustration, figure 5(a) shows how the values of χ^2 vary with c_{11} and c_{12} when c_{44} is pre-set to 128 GPa. It is seen that χ^2 shows a minimum in a narrow range comprising a nearly straight line, represented by $c_{11} - c_{12} = 90$ GPa. Similar results are obtained with c_{44} preset to 126 or 128 GPa. The results indicate that the SAW velocity data are only sensitive to the elastic constant c_{44} and the combination $c_{11} - c_{12}$. To corroborate

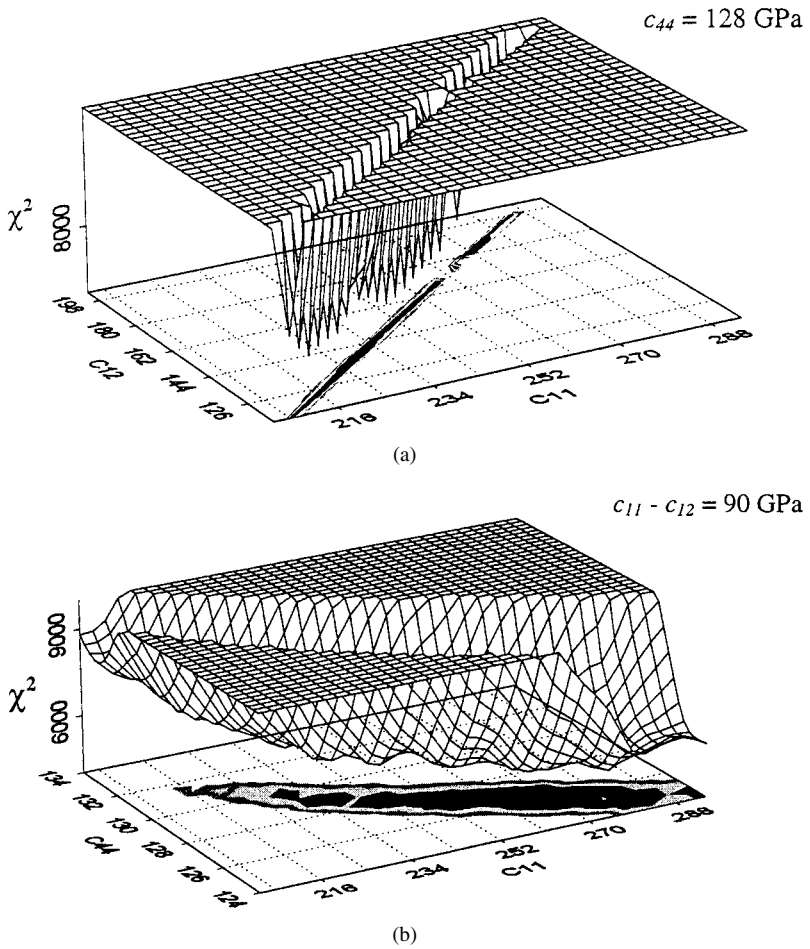

Figure 5. (a) Three dimensional graph of χ^2 with variation of c_{11} and c_{12} for CMSX-4 from the SAW data alone. The elastic constant c_{44} is pre-set to 128 GPa. (b) Three dimensional graph of χ^2 with variation of c_{11} and c_{44} for CMSX-4 from the SAW data alone. The elastic constant combination $(c_{11} - c_{12})$ is pre-set to 90 GPa. In both cases the minimum is ill defined.

this conclusion, the values of $c_{11} - c_{12}$ were preset to 88, 90 and 92 GPa, respectively, and c_{11} and c_{44} were varied. As illustrated in figure 5(b) for $c_{11} - c_{12} = 90$ GPa, χ^2 shows an extended valley with $c_{44} = 127 \pm 3$ GPa and $c_{11} = 250 \pm 30$ GPa. The uncertainty in c_{44} of about 2.4% is acceptable in view of the inherent measurement errors, but the uncertainty in c_{11} is substantial, being about 12%. With $c_{11} - c_{12}$ preset to 88 or 92 GPa, the minima in χ^2 become extended and yield an unrealistic range of values for c_{11}. The results confirm that analysis of the Rayleigh and p-SAW data of angular variation of velocity, while being sensitive to the elastic constant c_{44} and the combination $c_{11} - c_{12}$, is inadequate to provide the full set of independent elastic constants.

4.2.2. Use of the continuum of surface modes. As discussed in section 2, the continuum of bulk excitations leading to the Lamb shoulder in SBS spectra identifies the slow transverse and longitudinal bulk wave thresholds associated with lateral waves. Their respective velocities,

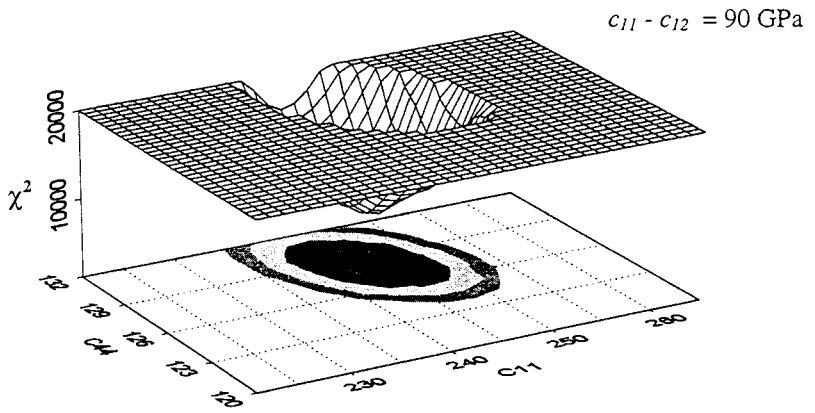

Figure 6. Three dimensional graph of the variation of χ^2 with c_{11} and c_{12} for CMSX-4 using the combined data of the angular variation of SAW velocity and the Lamb shoulders. The elastic constant combination $(c_{11} - c_{12})$ is pre-set to 90 GPa. The minimum is well defined.

determined from the corresponding frequencies measured by SBS, can provide direct values of the elastic constants or their combinations.

In order to make use of this method successfully the surface quality of the specimen and the sensitivity of the detector need to be sufficiently high to produce an adequate signal to noise ratio in the region of the Lamb shoulder. The results of long-period scans are shown in figure 2, in which the anti-Stokes SBS spectra of CMSX-4 for the [100] and [110] directions on the (001) surface are shown as a function of phase velocity. For each spectrum, in addition to the dominant SAW peak, the Lamb shoulder with its transverse and longitudinal thresholds is shown. In the present work the longitudinal thresholds were used, these corresponding to the well defined minima in the Lamb shoulder in the region between 5 and 6 km s^{-1}. The following values for the elastic constants, or their combinations, emerged from the relations given in section 2 for these thresholds corresponding to the [100] and [110] directions, respectively: $c_{11} = 242$ GPa obtained for the [100] direction and $c_{11} + c_{12} + 2c_{44} = 661$ GPa obtained from the [110] direction.

These additional two measurements provide the necessary sensitivity to the value of c_{11} such that, in combination with the SAW angular dispersion data, all three elastic constants are successfully recovered. The minimization of

$$\chi^2 = \sum_{SAWs} (V_i^{meas} - V_i^{calc})^2 + \sum_{L} (V_i^{meas} - V_i^{calc})^2$$

with respect to variations of the elastic constants was carried out, where the V_i^{calc} are the velocities determined from the surface Green function for the RW and p-SAW, respectively, over the range of α angles measured, and for the two minima in the Lamb continuum (L). Figure 6 shows the variation in χ^2 as a function of c_{11} and c_{44} for a fixed value of $(c_{11} - c_{12})$. The minimum in χ^2 is well defined, unlike the situation in figures 5(a) and 5(b). The analysis yielded satisfactory ambient temperature elastic constants, namely: $c_{11} = 243 \pm 2$ GPa; $c_{12} = 153 \pm 2$ GPa and $c_{44} = 128 \pm 1$ GPa.

Elastic constants or their combinations can be obtained directly from measurements of the Lamb shoulder and the respective SAW peak for appropriate symmetry directions [100] and [110] without the need for the measurements of the full angular dispersion of the RW and/or the p-SAW as discussed in section 2. To verify the procedure, the value of χ^2 was calculated with variation in all three elastic constants. As an example, figure 7 shows a contour plot of

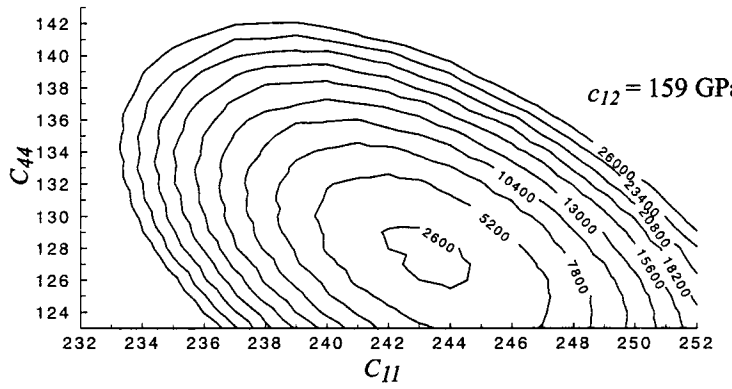

Figure 7. Contour plots of the variation of χ^2 with c_{11} and c_{44} for CMSX-4 from the combined data of the respective minima corresponding to the longitudinal threshold in the Lamb shoulder for the [100] and [110] directions of the (001) plane and the positions of the respective SAW peaks. The elastic constant c_{12} is pre-set to 159 GPa. The minimum is well defined and hence the three elastic constants can be determined.

the variation of χ^2 as a function of c_{11} and c_{44} with a preset values of $c_{12} = 159$ GPa, which yielded convergent contours and a well defined minimum in χ^2. The three elastic constants obtained, by this method are consistent with the results obtained from the combined data of the angular dispersion of the SAWs and the Lamb shoulder data discussed earlier, being $c_{11} = 243 \pm 2$ GPa, $c_{12} = 159 \pm 2$ GPa and $c_{44} = 127 \pm 1$ GPa.

4.3. High-temperature SBS measurements

SBS measurements were carried out on the CMSX-4 sample at temperatures to 600 °C in an optical furnace that permitted the sample to be rotated about the surface normal using a backscattering geometry. The design of the furnace was similar to that used by Stoddart *et al* [11] but incorporated the furnace heater winding outside the silica furnace tube in order to reduce contamination of the sample surface.

The evaluation of the elastic constants as a function of temperature made use of a combination of the methods discussed above. Since the measurement of the Lamb shoulder and the relevant SAW peak had proved adequate to determine the set of elastic constants at room temperature, careful measurements of the SBS spectrum were made for the surface wavevector in the [100] and [110] directions at 200 °C and 400 °C. At 600 °C, the surface quality of the sample deteriorated, which made the observation of the Lamb shoulder and the longitudinal threshold impossible. A full measurement of the angular dependence of the SAW velocities was carried out. Figure 8 shows the results with the room-temperature measurements included for comparison. The measured SAW velocities and the velocities determined from the longitudinal wave threshold within the Lamb shoulder for the [100] and [110] directions show a small linear decrease in each velocity with increasing temperature.

4.4. Evaluation of the room- and high-temperature elastic properties

It is instructive to compare the elastic constants and anisotropy ratio A obtained from our SBS measurements of CMSX-4 superalloy with those studies carried out at room temperature using other techniques. Table 2 shows the values obtained by a resonance method [19], a pulse echo technique [20] and by use of a scanning ultrasonic microprobe [21]. In general the values are in

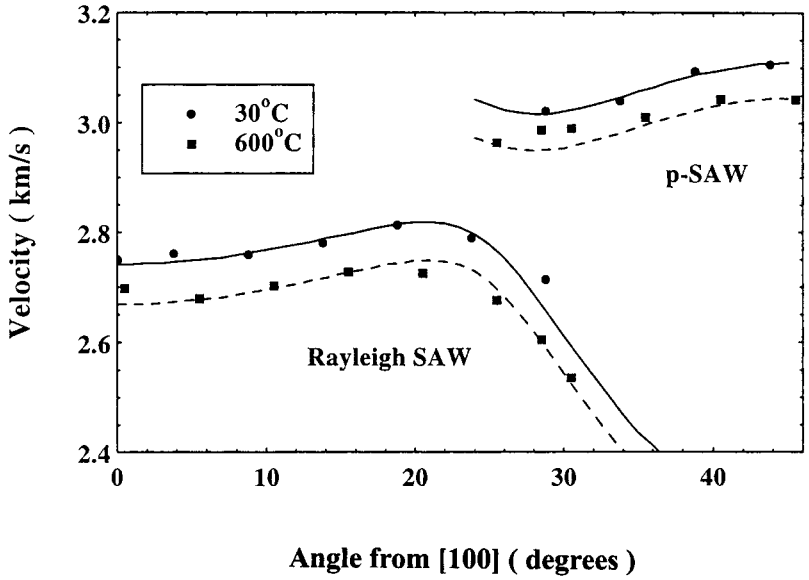

Figure 8. Direction dependence of the Rayleigh and p-SAW velocities for CMSX-4 at room temperature and 600 °C. The dispersion curve moves to lower velocities as the temperature increases.

Table 2. Measured room-temperature elastic constants and the anisotropy ratio A of CMSX-4 superalloy.

	c_{11}	c_{12}	c_{44}	$c_{11}-c_{12}$	A
Hermann [19]	251	159	132	92	2.87
Alberts [20]	248	155	132	93	2.84
Amulele [21]	258	159	129	89	2.61
Present work	243	153	128	90	2.84

quite good overall agreement, with the SBS results being slightly lower than those obtained by others. The most likely explanation is the presence of surface damage caused by mechanical polishing as suggested by Mendik *et al* [13].

Before the SBS spectra were obtained, it was not clear what effect the two-phase structure of the superalloy would have on the Brillouin spectra. The γ' microstructure typically has dimensions of the order of 1 μm, which is comparable to the acoustic wavelength ($\sim$270 nm). From the measured spectra, it appears that the two phases either form an effective medium for the acoustic waves, or that the elastic properties are sufficiently well matched that the two different scattering contributions cannot be resolved. Certainly for alloys such as CMSX-4 that are related to Ni_3Al, the elastic constants of the precipitate are usually only slightly different from those of the matrix [1].

Figure 9 shows the elastic constants of CMSX-4 as a function of temperature using the respective methods as discussed above. In the calculation of the elastic constants at the various temperatures the density was determined from the values of the thermal expansion coefficient, being 8.67, 8.60 and 8.51 $\times 10^3$ kg m^{-3}, respectively, at 200 °C, 400 °C and 600 °C [22]. Since only the angular variation of SAW velocities was measured at 600 °C, it was only possible to determine c_{44} to the required accuracy at this temperature. The values of all three elastic constants decrease linearly with increasing temperature in accord with the quasi-harmonic

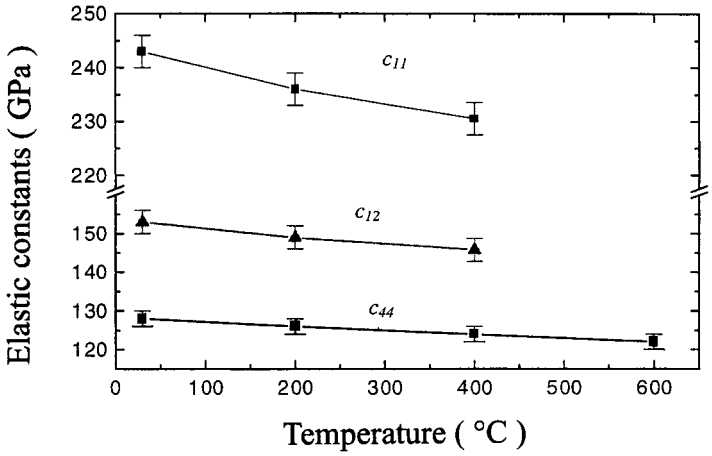

Figure 9. Variation of the elastic constants with temperature for CMSX-4. The elastic constants display a linear decrease with increasing temperature.

theory [23]. There is excellent agreement in the observed trends which confirms the degree of agreement between the various methods used for elastic constant determination.

Young's modulus E and the shear modulus G are widely used in engineering applications of superalloys as discussed in the introduction. These elastic moduli are expressed as directionally dependent combinations of the tensor elastic constants (Schmidt and Boas [24], Hertzberg [25]). Figure 10 shows the values of E and G in the three high-symmetry directions [100], [110] and [111] for CMSX-4 as a function of temperature. Both E and G are strongly direction dependent and decrease linearly with increasing temperature.

4.5. Features of the SBS spectra

Figures 2 and 3 show the experimental SBS spectra for different values of the angle α including the Rayleigh SAW and p-SAW peaks and features of the Lamb shoulder in considerable detail. Using the values of the elastic constants determined as described above, the theoretical spectra calculated by means of the surface Green function method and are in very good agreement with experiment. The shape of the Lamb shoulder, including the transverse and longitudinal thresholds, is correctly reproduced by theory. The calculated positions of the Rayleigh SAW (figure 2(a)) and the p-SAW (figure 2(b)) agree well with experiment. However the experimental peaks are instrumentally broadened.

In figure 3(b) for $\alpha = 40^\circ$ from the [100] direction, it is seen that in addition to the intense p-SAW peak, another weak broadened peak is present near 2.4 km s^{-1}. (The abrupt fall in intensity below 2.4 km s^{-1} in the experimental spectrum results from the chosen spectral position of the slow-scanning window of the interferometer.) For this surface wavevector direction, the scattering cross section of the Rayleigh SAW is very weak, and although a sharp peak is present in the calculated spectrum, its integrated intensity is very small. In the experimental spectrum, the weak Rayleigh peak cannot be resolved from the scattering of the slow transverse bulk wave (2.32 km s^{-1}).

In the SBS spectrum for $\alpha = 28^\circ$ from the [100] direction shown in figure 3(a), there is a second minimum in the Lamb shoulder corresponding to a velocity of about 3.6 km s^{-1}. The Green function calculation predicts this minimum well. The minimum corresponds to the fast transverse threshold.

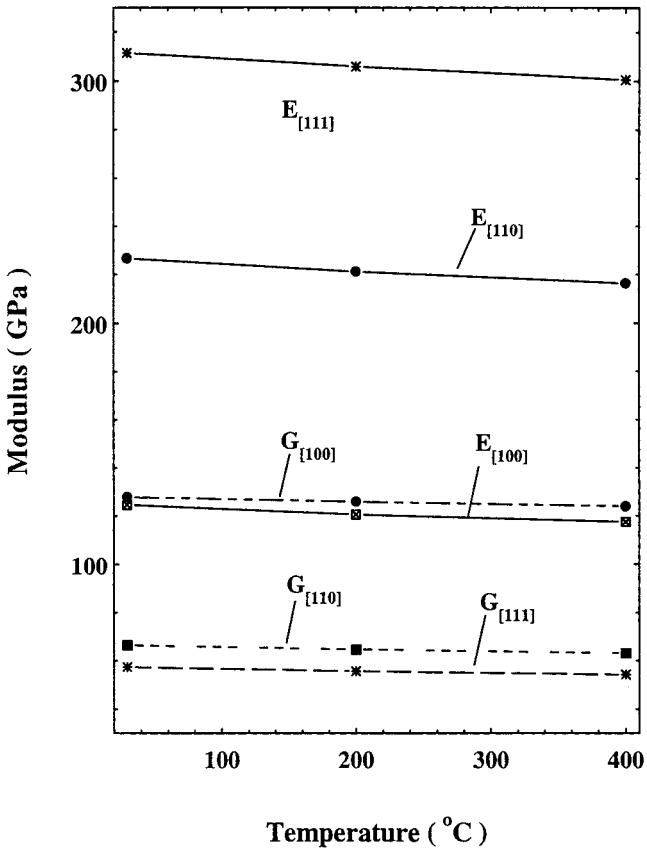

Figure 10. Variation of Young's modulus (E) and the shear modulus (G) with temperature for CMSX-4. Both moduli are strongly direction dependent and decrease linearly with increasing temperature.

In accounting for SBS spectra in general, it is necessary to consider the effects of both the surface ripple and elasto-optic mechanisms [26]. In the present case of the superalloy CMSX-4, being a highly opaque metal, the Green function method pertaining solely to the surface ripple mechanism yields results in very good agreement with the experimental spectra. We conclude that the contributions from the elasto-optic mechanism are very small.

5. Conclusions

SBS studies using both experimental and theoretical approaches have provided a detailed understanding of the thermally induced surface dynamics of the nickel-based superalloy CMSX-4 in the GHz frequency range. The wealth of features in the SBS spectrum has been accounted for in detail and these have been used to calculate the elastic constants in a variety of self-consistent ways. The elastic constants and engineering moduli have been measured at high temperatures, further demonstrating the potential of SBS in this regard.

Acknowledgment

We thank the National Research Foundation, Pretoria for financial support.

References

[1] Nabarro F R N and de Villiers H L 1995 *The Physics of Creep* (London: Taylor and Francis)
[2] Kear B H 1986 *Sci. Am.* **225** 59
[3] Kuhn H A and Sockel H G 1990 *Phys. Status Solidi* a **119** 93
[4] Bayerlein U and Sockel H G 1991 *Mater. Sci. Eng.* A **141** 179
[5] Hermann W, Sockel H G, Han J and Bertram A 1996 *Superalloys* ed R D Kissinger *et al* (Berlin: Minerals, Metals and Materials Society) p 229
[6] Nizzoli F and Sandercock J R 1990 Dynamical properties of solids *The Modern Physics of Phonons: Transport, Surfaces and Simulations* vol 6, ed G K Horton and A A Maradudin (Amsterdam: North-Holland) ch 5, p 281
[7] Mutti P, Bottani C E, Ghislotti G, Beghi M, Briggs G A D and Sandercock J R 1995 *Advances in Acoustic Microscopy* vol 1, ed A Briggs (New York: Plenum) p 249
[8] Comins J D 2001 *Handbook of Elastic Properties of Solids, Liquids and Gases* vol 1, ed A G Every and W Sachse (New York; Academic) ch 15
[9] Zhang X, Comins J D, Every A G, Stoddart P R, Pang W and Derry T D 1998 *Phys. Rev.* B **58** 13 677
[10] Stoddart P R, Comins J D and Every A G 1995 *Phys. Rev.* B **51** 17 574
[11] Stoddart P R, Comins J D and Every A G 1996 *Physica* B **219/220** 717
[12] Crowhurst J C, Hearne G R, Comins J D, Every A G and Stoddart P R 1999 *Phys. Rev.* B **60** R14 990
[13] Mendik M, Satish S, Kulik A, Gremaud A and Wachter P 1992 *J. Appl. Phys.* **71** 2830
[14] Sklar Z, Mutti P, Stoodley N C and Briggs G A D 1995 *Advances in Acoustic Microscopy* vol 1, ed A Briggs (New York: Plenum) p 209
[15] Mock R and Güntherodt G 1984 *J. Phys. C: Solid State Phys.* **17** 5635
[16] Comins J D, Every A G, Stoddart P R, Zhang X, Crowhurst J C and Hearne G R 2000 *Ultrasonics* **38** 450
[17] Stoddart P R, Crowhurst J C, Every A G and Comins J D 1998 *J. Opt. Soc. Am.* B **15** 2481
[18] Farnell G W 1970 *Physical Acoustics* vol 6, ed W P Mason and R W Thurston (New York: Academic) p 109
[19] Hermann W 1988 personal communication
[20] Alberts V 1998 personal communication
[21] Amulele G M, Every A G and Yates S C 1999 *Review of Progress in Quantitative NDE* vol 18, ed D O Thompson and D E Chimenti (New York: Kluwer–Plenum) p 2001
[22] Yates S C 1997 personal communication
[23] Garber J A and Granato A V 1975 *Phys. Rev.* B **11** 3990
[24] Schmidt E and Boas W 1950 *Plasticity of Crystals* (London: Hughes)
[25] Hertzberg R W 1989 *Deformation and Fracture Mechanics of Engineering Materials* 3rd edn (New York: Wiley)
[26] Bassoli L, Nizzoli F and Sandercock J R 1986 *Phys. Rev.* B **34** 1296